Engineering Fracture Mechanics xxx (2012) xxx–xxx

Contents lists available at SciVerse ScienceDirect

Engineering Fracture Mechanics

journal homepage: www.elsevier.com/locate/engfracmech

Full field measurements of anisotropic stress intensity factor ranges in fatigue

Garrett J. Pataky [a], Michael D. Sangid [b], Huseyin Sehitoglu [a,*], Reginald F. Hamilton [c], Hans J. Maier [d], Petros Sofronis [a]

[a] Department of Mechanical Science and Engineering, University of Illinois at Urbana–Champaign, 1206 W. Green St., Urbana, IL 61801, USA
[b] School of Aeronautics and Astronautics, Purdue University, 701 W. Stadium Ave., West Lafayette, IN 47907-2045, USA
[c] Department of Engineering Science and Mechanics, Pennsylvania State University, 212 Earth-Engineering Sciences Building, University Park, PA 16802-6812, USA
[d] Lehrstuhl für Werkstoffkunde (Materials Science), University of Paderborn, 33095 Paderborn, Germany

ARTICLE INFO

Article history:
Received 21 February 2012
Received in revised form 29 May 2012
Accepted 5 June 2012
Available online xxxx

Keywords:
Fatigue crack growth
Effective stress intensity factor
Mixed mode fracture
Plastic zones
Slip irreversibility

ABSTRACT

The effects of anisotropy during mixed mode fatigue crack growth were studied in single crystal 316L stainless steel. An anisotropic least-squares regression algorithm using displacements from digital image correlation was developed to find the effective stress intensity factors, K_I and K_{II}, and the T-stress. Crack tip plastic zones were determined using an anisotropic yield criterion. Strains in the plastic zone obtained from digital image correlation showed a dependence on the crystallography and load ratio. Crack tip slip irreversibility was measured and showed an increasing trend with increasing crack length; this information is critical for describing crack growth behavior.

1. Introduction

Fatigue crack growth has been studied extensively, since the risk of crack propagation is one of the largest detriments to the life of engineering components. The majority of these studies have focused on the tensile opening of cracks, i.e. mode I growth. Forsyth recognized Stage I cracks grow at an angle, introducing the need to study mode II growth [1]. Work followed considering more than pure mode I crack growth and combinations of mixed mode stress intensity factors were used to describe mixed mode crack growth [2]. It has been found that mode II growth has a large impact on crack initiation and early crack growth within individual grains of a polycrystalline aggregate [3]. This is due to plastic deformation during fatigue cycling, which concentrates on the slip systems experiencing the maximum shear stress [4]. As investigations were extended to rolling contact fatigue, commonly seen in the railroad industry, it became necessary to include the mode II growth of cracks beyond the Stage I growth [5,6]. This need to understand both Stage I and Stage II was also observed during the study of nickel-based alloy single crystals [7]. Single crystals have been utilized in this study to better understand the plastic strains present in a single grain during mixed mode (I and II) fatigue crack growth. One of the key features of our study is that we extract anisotropic stress intensity factors, K_I *and* K_{II}, from displacements utilizing special algorithms, thus allowing accurate characterization and analysis of mixed mode crack growth.

Fracture mechanics has shown that the stress and displacement fields around the crack tip singularity are important for describing the crack driving forces. In 1957, Williams first determined the stress fields around a crack tip in an elastic, isotropic body using an infinite power series and found the first term to be of the order $r^{-1/2}$, where r is the radial distance

* Corresponding author.
E-mail address: huseyin@illinois.edu (H. Sehitoglu).

0013-7944/$ - see front matter © 2012 Elsevier Ltd. All rights reserved.
http://dx.doi.org/10.1016/j.engfracmech.2012.06.002

Nomenclature

a_{ij}	elastic constants
A	rigid body rotation
B_u	horizontal rigid body translation
B_v	vertical rigid body translation
C	Paris law coefficient
K_I	mode I stress intensity factor
K_{II}	mode II stress intensity factor
ΔK_I	mode I stress intensity factor range
ΔK_{II}	mode II stress intensity factor range
$\Delta K_{I,eff}$	mode I effective stress intensity factor range
$\Delta K_{II,eff}$	mode II effective stress intensity factor range
ΔK_{tot}	combined mode I and mode II stress intensity factor ranges
m	Paris law exponent
r	radial distance from crack tip
r_p	plastic zone radius
R	load ratio
T	T-stress term
u	horizontal displacements
v	vertical displacements
X, Y, Z	yield stresses in the principle directions
S	yield stress in the shear direction
α	energy release rate ratio factor
$\Im_i$	mode i energy release rate
θ	the angular coordinate from the crack tip
σ_x, σ_y	stress in the x and y directions respectfully
τ_{xy}	shear stress in the x–y plane

from the crack tip. The T-stress term is the second term in this expansion [8]. Sih et al. used a similar analysis for an anisotropic body and solved the general equations for those crack tip stresses, finding the stress singularities to be of the same order [9]. Both of these solutions consider mode I, mode II, and anti-plane, or mode III, loading.

Crack initiation during fatigue typically begins along an active slip system in a single grain within a polycrystalline material; this active slip system corresponds with the plane of maximum resolved shear stress range. This shearing crack growth is referred to as mode II. After some growth, the crack tends to turn towards the plane of maximum tensile stress or mode I growth [10]. This process is highly dependent on crystallography, and thus single crystals are utilized to study early crack growth in the present work. Using single crystals also removes grain boundary effects on fatigue crack growth. In an fcc material, such as the 316L stainless steel used in this study, desired testing conditions can be achieved with knowledge of the slip planes. For instance, a [1 1 1] oriented crystal with a single notch in the [2 $\bar{1}$ $\bar{1}$] direction with a far field uniaxial loading will initiate and grow an angled crack on the {111} plane which will experience local mixed mode loading along the crack flanks.

Once it became evident that mode II loading contributed to fatigue crack growth, more studies were aimed at investigating mixed mode loading. Rybicki and Kanninen used the finite element method in conjunction with the crack closure integral to solve for the effective mode I and mode II stress intensity factors [11]. This was followed by another finite element analysis produced by Nakagaki and Atluri of a crack experiencing mixed mode loading. They found that crack closure occurred at nodes away from the crack tip as well [12]. In other studies, mode II was found to dominate the crack growth behavior when the cyclic stress had a strong compression load associated with it [10]. This was an early indication that the load ratio, R, played a role in the magnitude of mode II growth. By comparing the stress intensity factor ranges, ΔK, associated with each mode, it was concluded that when the value of $\Delta K_{II}/\Delta K_I$ was high, the crack grew in shear, and when this ratio was low the crack grew in tension [10].

Research has also focused on crack flank displacements and the associated mode II crack growth. Smith and Smith found that mode II displacements start at the notch and described the crack as sliding [13]. A crack was only sliding until the shear displacements reached the crack tip, and then the crack was considered to be fully slid. Sliding was also defined to be reversed if it fully occurred during both the loading and unloading of a fatigue cycle [13]. Kibey et al. used a finite element model to simulate the crack closure of an inclined crack subject to a remote tensile (mode I) loading [14]. Slanted cracks experience mixed mode loading allowing for the study of mode I and mode II crack opening levels. It was noted that a load ratio with a compressive load experienced earlier opening in both modes I and II as compared to a purely tensile load ratio. The maximum stress and friction between the crack faces also affected the opening levels.

The use of digital image correlation (DIC) during fatigue crack growth studies enables the use of displacements to extract the stress intensity factors during a loading cycle. One DIC technique introduced for fatigue crack growth studies was a two-

Please cite this article in press as: Pataky GJ et al. Full field measurements of anisotropic stress intensity factor ranges in fatigue. Engng Fract Mech (2012), http://dx.doi.org/10.1016/j.engfracmech.2012.06.002

point digital image correlation displacement gage used to measure the local crack opening displacement [15,16]. McNeill et al. introduced the idea of using DIC displacements to find stress intensity factors [17]. Carroll et al. compared several methods which determined the mode I stress intensity factor, K_I, the value of the T-stress, and the level of crack closure [18]. T-stress is the second term in the Williams expansion and represents the uniform stress component, which is parallel to the crack [19]. Recently, a study used DIC and a least-squares regression when studying isotropic mixed mode fatigue crack growth and measured K_I and K_{II} values [20]. DIC has been employed to focus on crack kinking in functionally graded materials [21]. These materials still exhibited isotropic properties, and the authors were able to determine K_I, K_{II}, and the T-stress. Another significant aspect of these techniques was that since they were based on experimental displacements, crack closure was included; therefore, the effective stress intensity factors were found.

A crack represents a singular point of stress concentration within a material and therefore yields the surrounding grains and introduces localized plasticity ahead of the crack tip. The plastic strains accumulated during cyclic loading with a crack present are known to form a plastic zone extending from the crack tip [22]. The plastic zone size can be estimated by determining at which point the stresses ahead of the crack tip meet the yield criterion. In the case of an isotropic body under pure mode I loading, the plastic zone has been observed to be symmetric. In the case of combined mode I and mode II loading, such as that found in an anisotropic body, the plastic zone is asymmetric [23,24]. As previously mentioned, inclined cracks can experience mixed mode crack growth. The angle of this inclination has also been shown to have an effect on the plastic zone shape [25,26].

The stress intensity factors, K_I and K_{II}, can be used to describe the size and shape of the plastic zone. Gao et al. concluded that beginning at moderate stress levels, the T-stress term becomes significant in the crack tip stress field, and influence the plastic zone size [27]. Betegon and Hancock concurred and found that the T-stress can also influence the plastic zone shape. Inside this plastically deformed area is a reversed plastic zone [28]. This reversed plastic zone experiences reversed plasticity upon unloading during a fatigue cycle. McClung and Sehitoglu found that the size of the reversed crack tip plastic zone can be affected by the amount of crack closure [29]. In 1968, Tomkins was the first to correlate crack tip plasticity to the crack growth rate [30]. Several authors extended this conclusion and focused on the strains in the reversed plastic zone. This led to the finding that an increase in the magnitude of the plastic strains inside the reversed plastic zone correlated with an increase in the crack growth rate [27,31]. A further refinement was the suggestion that irreversibility of slip ahead of the crack tip contributed to the fatigue crack growth behavior. McEvily and Boettner observed slip in polycrystalline (copper-based alloys) and single crystal (aluminum) specimens and concluded crack propagation was related to cross slip [32]. Building upon this idea, Fong and Tromans proposed a restricted slip reversal model relating slip irreversibility to crack growth [33]. Expansions on this model include relating plastic strain ahead of the crack tip due to slip irreversibility to the crack growth rate [34].

The following study gives insight into mixed mode fatigue crack growth in single crystal 316L stainless steel, which is crucial to understanding complicated crack propagation in individual grains of an alloy. Displacements obtained using digital image correlation were used to determine the crack driving forces occurring during a fatigue cycle and to characterize the plastic zone strains. The first section of the paper discusses the materials and equipment employed for the experimental testing. The analysis sections discuss the least-squares regression used to extract the crack tip stress field information from the DIC results and the calculations of the plastic zone size and shape. The results show the strain development and irreversible strains produced during a mixed mode I and mode II fatigue crack cycle. A stress intensity factor measurement technique for anisotropic specimens of any geometry was developed and slip irreversibility was quantitatively found to increase with crack length.

2. Materials and experimental procedure

Commercially available 316L stainless steel was used for testing. A portion of the material was grown into a single crystal from a seed using the Bridgman technique in vacuum. The orientation of this crystal was then determined using electron backscatter diffraction (EBSD) enabling slices parallel to the $\{1\bar{1}0\}$ plane to be cut. This plane contains the two crystallographic orientations of interest, [001] *and* [111]. The polycrystalline material and both of the single crystal orientations were used during the study. Single edge-notch tension specimens were electrical discharge machined (EDM) with a gage length of 9 mm long, a width of 3 mm, and a notch depth of 0.5 mm with the thicknesses reported in Table 1.

The specimens were polished to a mirror finish using abrasive paper. Black paint was then airbrushed onto each specimen to create a speckle pattern for digital image correlation (DIC). For a description of the digital image correlation technique, see [35,36]. A digital camera was used to capture images during the fatigue crack growth experiments. The camera resolution

Table 1
Summary of the specimen dimensions, testing conditions, and equipment setup.

Crystallography (orientation)	Thickness (mm)	*R* ratio	Stress range (MPa)	Magnification	Resolution (μm/pix)	Measurement cycle frequency (Hz)	Images per cycle
Polycrystalline	1.23	0.0624	245	4.9×	0.90	1	15
[111]	1.03	0.05	178	4.6×	0.95	1	15
[111]	1.75	−1	300	6×	0.78	0.08	188
[001]	1.08	0.05	155	5.1×	0.85	0.25	60

Please cite this article in press as: Pataky GJ et al. Full field measurements of anisotropic stress intensity factor ranges in fatigue. Engng Fract Mech (2012), http://dx.doi.org/10.1016/j.engfracmech.2012.06.002

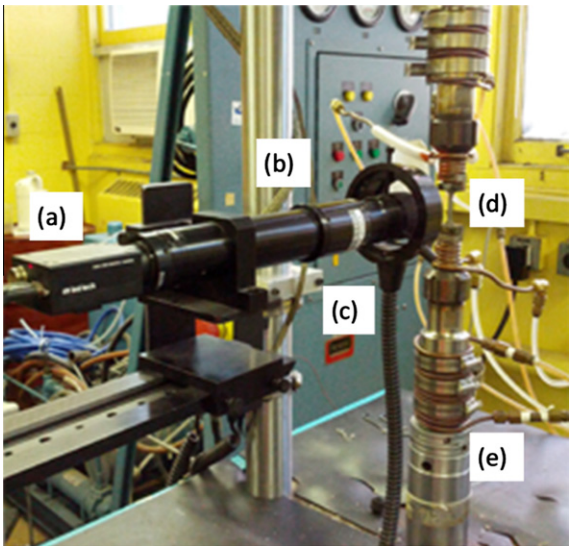

Fig. 1. The experimental setup. Labeled in the figure: (a) camera, (b) lens, (c) light source, (d) specimen, and (e) load frame.

was 1600 by 1200 pixels, the maximum frame rate was 15 fps, and an adjustable lens with a 12× magnification range and 2× adapter were used to achieve different magnifications. The experimental setup is shown in Fig. 1. The magnification and resolution of the images for each specimen are displayed in Table 1. The specimens were loaded in fatigue at the *R*-ratios and stress ranges given in Table 1 at a rate between 3 and 10 Hz to initiate a crack at the notch. A computer program controlled the servo-hydraulic load frame, and captured images and their corresponding loads measured by a 7.5 kN load cell during the test. Once a crack was visually identified, measurement cycles were run periodically to capture a greater number of images per cycle to provide an in-depth analysis into the fatigue cycles.

A commercially available image correlation program was used to perform DIC analysis. The first image of each measurement cycle, captured at minimum load, was used as the reference image for that cycle. The full field of the image, both behind and ahead of the crack tip, was used for correlations. A two-point digital image correlation displacement gage (digital extensometer), which consists of a subset on each crack flank, was used to measure crack opening displacements; multiple digital extensometers were placed on the image along the length of the crack spanning from the crack tip to the notch [15,16]. The maximum subset size used was 72 by 72 μm with a maximum of 9 μm between centers of the subsets. Each extensometer provided, the horizontal (u) and vertical (v) displacements and the strains were calculated assuming a small strain approximation. The displacements are used in the least-squares regression as discussed in Section 3.

After testing, electron backscatter diffraction (EBSD) was performed on the single crystal specimens to verify their orientations. For the two [1 1 1] crystals, their loading directions were confirmed, the normal was determined to be $[0\,\bar{1}\,1]$, and thus the third orientation $[2\,\bar{1}\,\bar{1}]$. The [0 0 1] crystal was also confirmed to be properly oriented in the loading direction, the normal plane was $[1\,\bar{1}\,0]$, and the third orientation was $[\bar{1}\,\bar{1}\,0]$. A post fracture SEM micrograph of one of the [111] crystals is shown in Fig. 2. A schematic of the sample indicating the loading directions in crystal frame and the {111} slip planes in grey is shown in Fig. 3. The blue planes indicate the crack growth plane for each sample.

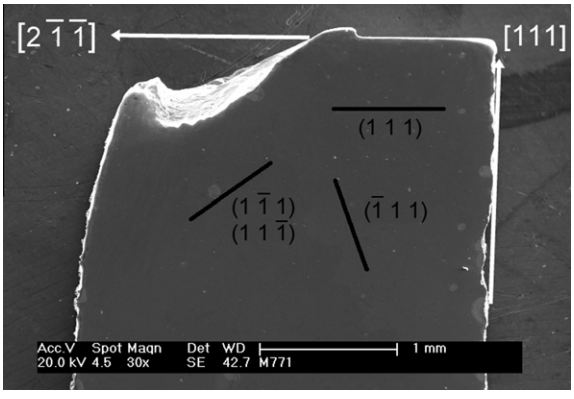

Fig. 2. SEM image of the [1 1 1] oriented single crystal specimen with the crystallographic orientations and the possible crack growth planes indicated.

Please cite this article in press as: Pataky GJ et al. Full field measurements of anisotropic stress intensity factor ranges in fatigue. Engng Fract Mech (2012), http://dx.doi.org/10.1016/j.engfracmech.2012.06.002

3. Regression analysis

The use of DIC provides a full field displacement field to find the crack driving forces without geometric considerations. A nonlinear least-squares regression can optimize the stress intensity factor determination process and give insight into how these values progress during a fatigue loading cycle. The following procedure describes how the stress intensity factors and higher order terms were found.

Since the frequency during the measurement cycles was slowed to the values given in Table 1, the entire loading and unloading process was recorded, and DIC provided a full field of displacements for each image. These displacements were the input to find K_I, K_{II}, and the T-stress. For mode I and mode II mixed mode crack problems, the crack tip displacements for an orthotropic material with the crack growth direction and crystallographic orientations consistent, as shown in Fig. 4 where the mechanical properties for $[h'\,k'\,l']$ are used instead of the loading direction $[h\,k\,l]$ properties, are expressed as [9,37]

$$u = K_I\sqrt{\frac{2r}{\pi}}\mathrm{Re}\left[\frac{1}{\mu_1-\mu_2}\left\{\mu_1 p_2\sqrt{\cos\theta+\mu_2\sin\theta}-\mu_2 p_1\sqrt{\cos\theta+\mu_1\sin\theta}\right\}\right]+K_{II} \times\sqrt{\frac{2r}{\pi}}\mathrm{Re}\left[\frac{1}{\mu_1-\mu_2}\left\{p_2\sqrt{\cos\theta+\mu_2\sin\theta}-p_1\sqrt{\cos\theta+\mu_1\sin\theta}\right\}\right]+a_{11}Tr\cos\theta+Ar\sin\theta+B_u \tag{1}$$

$$v = K_I\sqrt{\frac{2r}{\pi}}\mathrm{Re}\left[\frac{1}{\mu_1-\mu_2}\left\{\mu_1 q_2\sqrt{\cos\theta+\mu_2\sin\theta}-\mu_2 q_1\sqrt{\cos\theta+\mu_1\sin\theta}\right\}\right]+K_{II} \times\sqrt{\frac{2r}{\pi}}\mathrm{Re}\left[\frac{1}{\mu_1-\mu_2}\left\{q_2\sqrt{\cos\theta+\mu_2\sin\theta}-q_1\sqrt{\cos\theta+\mu_1\sin\theta}\right\}\right]+a_{12}Tr\sin\theta+Ar\cos\theta+B_v \tag{2}$$

where Re denotes the real part of a complex number,

$$p_j = a_{11}\mu_j^2+a_{12}-a_{16}\mu_j, \tag{3}$$

$$q_j = a_{12}\mu_j+\frac{a_{22}}{\mu_j}-a_{26}, \tag{4}$$

K_I and K_{II} are the mode I and mode II stress intensity factors respectively, T is the T-stress, A is the rigid body rotation, B_u and B_v are the rigid body translations in the u and v directions respectively, r and θ are the polar coordinates with the origin at the crack tip, μ_1 and μ_2 are the roots from the following characteristic Eq. (5), and a_{ij} are the elastic constants as found by Ledbetter for 316L stainless steel [38]. These two μ's are the two complex conjugate roots for which the imaginary parts are positive.

$$a_{11}\mu^4-2a_{16}\mu^3+(2a_{12}+a_{66})\mu^2-2a_{26}\mu+a_{22}=0 \tag{5}$$

In Eq. (2), the vertical displacements responsible for the tensile (mode I) crack opening are perpendicular to the crack surface. To accommodate this, the grid of displacements obtained from DIC and the compliance tensor values were rotated with respect to the crack propagation angle. This provides two distinct sets of experimental data: the horizontal displacements and the vertical displacements. An algorithm was written to simultaneously solve every vertical and horizontal displacement using Eqs. (1) and (2) for the desired parameters (K_I, K_{II}, T, A, B_u, B_v) using a nonlinear least squares regression. This provided the stress intensity factors values and T-stress directly from the experimentally measured displacement field without any contributions from the rigid motion. With the full field being used, over 10,000 displacements were considered in each calculation. It was deemed necessary during the development of the algorithm that both the horizontal and vertical displacements were required. If only the horizontal displacements, Eq. (1), were used, K_I is underestimated and K_{II} is overestimated. Contrary to this, if only the vertical displacements, Eq. (2), were used, K_I is overestimated and K_{II} is underestimated. This was due to the dominance of each stress intensity factor with its respective mode of opening; K_I when considering only the vertical displacements (mode I) and K_{II} when considering only the horizontal displacements (mode II).

4. Crack tip plastic zone analysis

With the stress intensity factors for mode I and mode II known, the stress field, Eq. (6), around the crack tip was determined [9]. The stress field was used to determine the plastic zone size and shape. The stresses are

$$\left.\begin{aligned}\sigma_x &= \frac{K_I}{\sqrt{2\pi r}}(F_{Ix}+mF_{IIx})\\ \sigma_y &= \frac{K_I}{\sqrt{2\pi r}}(F_{Iy}+mF_{IIy})\\ \tau_{xy} &= \frac{K_I}{\sqrt{2\pi r}}(F_{Ixy}+mF_{IIxy})\end{aligned}\right\}, \tag{6}$$

and the F terms in Eq. (6) are expressed as

Please cite this article in press as: Pataky GJ et al. Full field measurements of anisotropic stress intensity factor ranges in fatigue. Engng Fract Mech (2012), http://dx.doi.org/10.1016/j.engfracmech.2012.06.002

$$\left.\begin{aligned} F_{Ix} &= \mathrm{Re}\left[\frac{\mu_1\mu_2}{\mu_1-\mu_2}\left(\frac{\mu_2}{\sqrt{\cos\theta+\mu_2\sin\theta}}-\frac{\mu_1}{\sqrt{\cos\theta+\mu_1\sin\theta}}\right)\right] \\ F_{Iy} &= \mathrm{Re}\left[\frac{1}{\mu_1-\mu_2}\left(\frac{\mu_1}{\sqrt{\cos\theta+\mu_2\sin\theta}}-\frac{\mu_2}{\sqrt{\cos\theta+\mu_1\sin\theta}}\right)\right] \\ F_{Ixy} &= \mathrm{Re}\left[\frac{\mu_1\mu_2}{\mu_1-\mu_2}\left(\frac{1}{\sqrt{\cos\theta+\mu_1\sin\theta}}-\frac{1}{\sqrt{\cos\theta+\mu_2\sin\theta}}\right)\right] \end{aligned}\right\} \tag{7}$$

$$\left.\begin{aligned} F_{IIx} &= \mathrm{Re}\left[\frac{1}{\mu_1-\mu_2}\left(\frac{\mu_2^2}{\sqrt{\cos\theta+\mu_2\sin\theta}}-\frac{\mu_1^2}{\sqrt{\cos\theta+\mu_1\sin\theta}}\right)\right] \\ F_{IIy} &= \mathrm{Re}\left[\frac{1}{\mu_1-\mu_2}\left(\frac{1}{\sqrt{\cos\theta+\mu_2\sin\theta}}-\frac{1}{\sqrt{\cos\theta+\mu_1\sin\theta}}\right)\right] \\ F_{IIxy} &= \mathrm{Re}\left[\frac{1}{\mu_1-\mu_2}\left(\frac{\mu_1}{\sqrt{\cos\theta+\mu_1\sin\theta}}-\frac{\mu_2}{\sqrt{\cos\theta+\mu_2\sin\theta}}\right)\right] \end{aligned}\right\} \tag{8}$$

where $m = K_{II}/K_I$.

Since the single crystals exhibit anisotropic properties, Hill's extension of the von Mises's yield criterion was used [39]. The yield criterion in quadratic form is expressed as

$$E(\sigma_y-\sigma_z)^2+G(\sigma_y-\sigma_x)^2+H(\sigma_x-\sigma_y)^2+2L\tau_{yz}^2+2M\tau_{xz}^2+2N\tau_{xy}^2=1 \tag{9}$$

$$\left.\begin{aligned} 2E &= \frac{-1}{X^2}+\frac{1}{Y^2}+\frac{1}{Z^2} \\ 2G &= \frac{1}{X^2}-\frac{1}{Y^2}+\frac{1}{Z^2} \\ 2H &= \frac{1}{X^2}+\frac{1}{Y^2}-\frac{1}{Z^2} \\ 2N &= \frac{1}{S^2} \end{aligned}\right\} \tag{10}$$

where E, G, and H are coefficients that characterize the anisotropy in the normal directions and L, M, and N are the coefficients that characterize the shear anisotropy. X, Y, and Z are the yield stresses in the principal directions and S is the shear yield stress. Assuming plane stress since the specimens are thin, $\sigma_z = \tau_{xy} = \tau_{yz} = 0$ and Eq. (9) reduces to

$$(G+H)\sigma_x^2-2H\sigma_x\sigma_y+(E+H)\sigma_y^2+2N\tau_{xy}=1 \tag{11}$$

To find the plastic zone size, we substituted Eq. (6) into Eq. (11) and solved for the plastic zone radius, r_p, with the final form:

$$r_p=\frac{K_I^2}{2\pi}\left\{(G+H)(F_{Ix}+mF_{IIx})^2-2H(F_{Ix}+mF_{IIx})(F_{Iy}+mF_{IIy})+(E+H)(F_{Iy}+mF_{IIy})^2+2N(F_{Ixy}+mF_{IIxy})^2\right\} \tag{12}$$

5. Results and discussion

Fatigue crack growth tests were performed on a polycrystalline specimen and the two previously discussed crystallographic orientations. The tensile properties for each are presented in Table 2. The crack growth behavior as a function of the total stress intensity factor range is given in Fig. 5a.

Several methods have been proposed for combining the stress intensity factor ranges [2]. The most general expression has the form

Table 2
Selected tensile properties of the 316L stainless steel specimens.

Crystallography (orientation)	Yield stress, 0.2% offset (MPa)	Elastic modulus (GPa)
Polycrystalline	230	192
[111]	466	329
[001]	329	121

Please cite this article in press as: Pataky GJ et al. Full field measurements of anisotropic stress intensity factor ranges in fatigue. Engng Fract Mech (2012), http://dx.doi.org/10.1016/j.engfracmech.2012.06.002

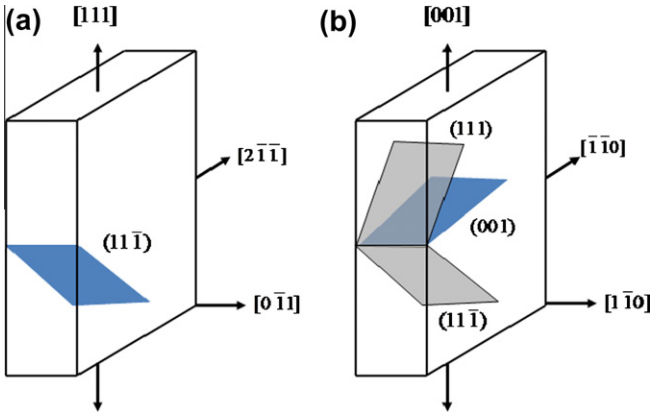

Fig. 3. A schematic of the samples in crystal frame showing the loading directions, {1 1 1} slip planes in gray, and the crack growth planes in blue.

Table 3
Paris law fits and stress intensity threshold from fatigue crack growth tests of 316L stainless steel.

Specimen	C	m
Polycrystal $R = 0.624$	2.46×10^{-09}	2.87
[1 1 1] Single crystal $R = 0.05$	9.96×10^{-13}	7.46
[1 1 1] Single crystal $R = -1$	7.86×10^{-13}	6.45
[0 0 1] Single crystal	6.50×10^{-12}	4.49

Table 4
Effective Paris law fits and stress intensity threshold from fatigue crack growth tests of 316L stainless steel.

Specimen	C	m
Polycrystal $R = 0.624$	1.05×10^{-08}	3.32
[1 1 1] Single crystal $R = 0.05$	6.37×10^{-09}	3.89
[1 1 1] Single crystal $R = -1$	3.29×10^{-09}	3.65
[0 0 1] Single crystal	3.10×10^{-09}	3.29

$$\Delta K_{tot} = \sqrt{(\Delta K_I)^2 + \alpha(\Delta K_{II})^2} \tag{13}$$

The anisotropic case has a more complex form and requires the use of the energy release rates, $\Im_i$, Eqs. (14) and (15), for mode I and mode II respectively [9]. The ratio between these two energy release rates will be used to determine α, i.e. $\Im_2/\Im_1$:

$$\Im_1 = -\frac{\pi K_I}{2} a_{22} \mathrm{Im}\left[\frac{K_I(\mu_1 + \mu_2) + K_{II}}{\mu_1 \mu_2}\right] \tag{14}$$

$$\Im_2 = \frac{\pi K_{II}}{2} a_{11} \mathrm{Im}\left[K_{II}(\mu_1 + \mu_2) + K_I \mu_1 \mu_2\right] \tag{15}$$

where a_{11} and a_{22} are the elastic constants. The α ranged from 2.25 to 3.8 for the cases included in this study.

The majority of the crack growth recorded occurred in regime II, the steady state region of fatigue crack growth. The experimental data were fit to the Paris law, Eq. (16), and the constants C and m are given in Table 3.

$$\frac{da}{dN} = C(\Delta K_{tot})^m = C\left[\Delta K_{I,eff}^2 + \alpha(\Delta K_{II,eff}^2)\right]^{m/2} \tag{16}$$

The crack growth behavior as a function of the effective total stress intensity factor range, for which crack closure is considered in the ΔK_{eff} calculation, is displayed in Fig. 5b. The effective mode I and mode II stress intensity factor ranges were determined for each test by utilizing the regression technique discussed in Section 3. Since the DIC displacements are the basis of this technique, crack closure during the fatigue cycle is inherently included. If there was no closure, the crack opening displacement magnitudes would be greater. These values were fit using Eq. (17) and the Paris fits for Fig. 5b are displayed in Table 4 and are similar to reported values [40].

$$\frac{da}{dN} = C(\Delta K_{tot,eff})^m = C\left[\Delta K_{I,eff}^2 + \alpha(\Delta K_{II,eff}^2)\right]^{m/2} \tag{17}$$

Please cite this article in press as: Pataky GJ et al. Full field measurements of anisotropic stress intensity factor ranges in fatigue. Engng Fract Mech (2012), http://dx.doi.org/10.1016/j.engfracmech.2012.06.002

5.1. The effective stress intensity factor range determination in the experiments

The regression analysis solves for each of the variables required to replicate the crack tip displacements during a fatigue crack growth cycle using Eqs. (1) and (2). These displacements will be referred to as the regressed displacements. The experimentally obtained and regressed displacements have been plotted together to demonstrate the accuracy of the regression technique. In Figs. 6–12, the blue[1] contours represent the experimentally found displacements and the red contours represent the regressed displacement contours. A selected fatigue cycle for each sample tested is presented at maximum load.

When the regression was performed on the polycrystalline specimen, isotropic compliance coefficients were used in Eq. (5). Since the crack was horizontal with no shear component, the mode II stress intensity factor range was nearly zero. The [0 0 1] oriented specimen also grew in pure mode I as expected because of symmetric slip with respect to the crack plane. As with the polycrystalline case, there was no mode II component, and thus the mode II stress intensity factor range was again nearly zero. The vertical displacements for the polycrystalline and [0 0 1] oriented specimen are given in Figs. 6 and 7 respectively. The experimental and regressed displacement contours show good agreement.

Two specimens with [1 1 1] orientations were tested to investigate mixed mode growth. The first [1 1 1] specimen was tested at a load ratio, R, of 0.05 as a comparison to the polycrystalline and [0 0 1] specimens. The horizontal and vertical displacement contours are displayed in Fig. 8a and b respectively for when the crack was 1.588 mm long. The mode I and mode II stress intensity factor ranges were determined to be 9.14 MPa $\sqrt{}$m and 4.33 MPa $\sqrt{}$m, respectively. The horizontal displacements are asymmetric in Fig. 8a. indicating shearing or mode II displacement is occurring during the cycle. A second test was conducted with the [1 1 1] orientation at a load ratio, R, of -1. With compression introduced into the fatigue cycle, the stress intensity factor ranges were expected to increase. The horizontal and vertical displacements for the cycle with crack length of 1.176 mm are displayed in Fig. 9a and b respectively. The mode I stress intensity factor range was 18.95 MPa $\sqrt{}$m and the mode II stress intensity factor range was 7.96 MPa $\sqrt{}$m. At a shorter crack length, it is already evident that the compressive part of the fatigue cycle had caused the stress intensity factors to increase by about a factor of two. The crack growth angle was within two degrees between both [1 1 1] specimens.

The importance of including crack closure when determining fatigue crack growth rates has been made evident in this section. Referring back to Fig. 5a, the fatigue crack growth results showed no consistency when using the isotropic (with no closure correction) stress intensity factor range calculation. When the crack closure was taken into account, the material, regardless of crystallography, demonstrated a common trend with the effective (anisotropic and close corrected) stress intensity factor ranges as shown in Fig. 5b. To elucidate this fact, Table 5 provides a brief comparison of five crack lengths between the effective and isotropic stress intensity factor ranges for the [1 1 1] oriented specimen with a load ratio, R, of 0.05. The mode I values show an average overestimation of 15%, and the mode II values show an average overestimation of 40%.

5.2. Plastic zone sizes

Since each image captured represents a different load throughout the fatigue cycle, the entire progression of stresses and strains was recorded. Using Eq. (12), the plastic zone size was determined using the stress intensity factors found in the regression analysis and the development of the size and shape throughout the fatigue cycle was observed. DIC was used to find the strains in front of the crack tip, and the strains inside the plastic zone are shown in Figs. 10–13 for the loading portion of a fatigue cycle up to maximum load for each specimen tested during this study.

The polycrystalline case presented in Fig. 10 displays the classic symmetric isotropic plastic zone shape for plane stress. At 6% of the load, the plastic zone is almost nonexistent with an area of 0.0007 mm^2. At the maximum load, the strains near the crack tip are greater than 1%, and extend out at roughly 60° from the crack tip with an area of 0.1920 mm^2. In the other pure mode I case, the [0 0 1] single crystal still has a symmetric plastic zone as shown in Fig. 11. At 29% of the load, the plastic

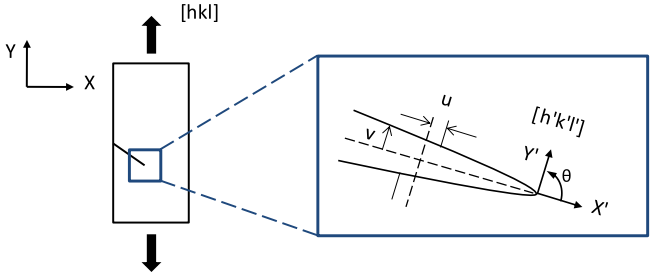

Fig. 4. Schematic showing the vertical (v) and horizontal (u) crack tip displacements, and the crystallographic orientation used.

[1] For interpretation of color in Figs. 3–10, the reader is referred to the web version of this article.

Please cite this article in press as: Pataky GJ et al. Full field measurements of anisotropic stress intensity factor ranges in fatigue. Engng Fract Mech (2012), http://dx.doi.org/10.1016/j.engfracmech.2012.06.002

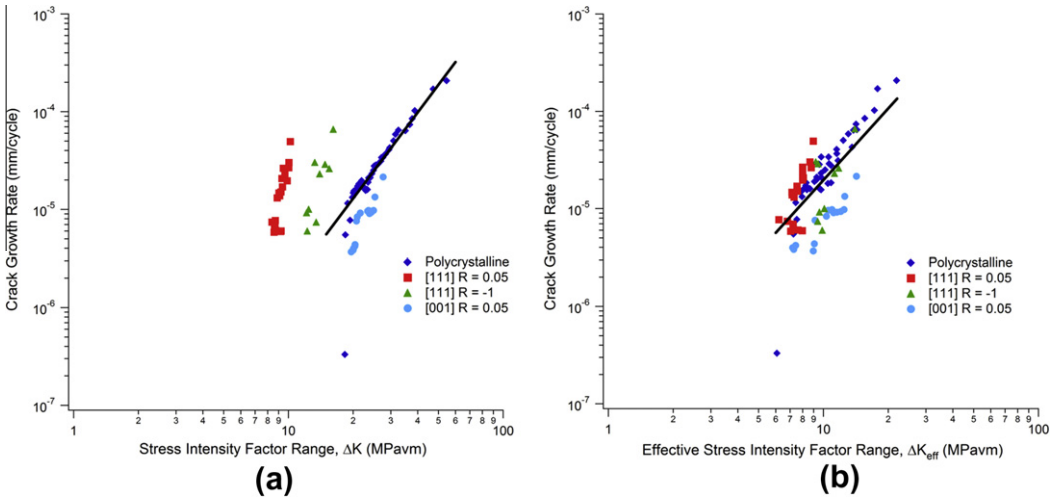

Fig. 5. Fatigue crack growth results for the polycrystalline and single crystal 316L stainless steel specimens at room temperature with testing conditions shown in Table 1. (a) Results based on the classical stress intensity factor range with the Paris law fits displayed in Table 3. (b) Effective fatigue crack growth results found using the least squares regression stress intensity factor ranges with Paris law fits given in Table 4.

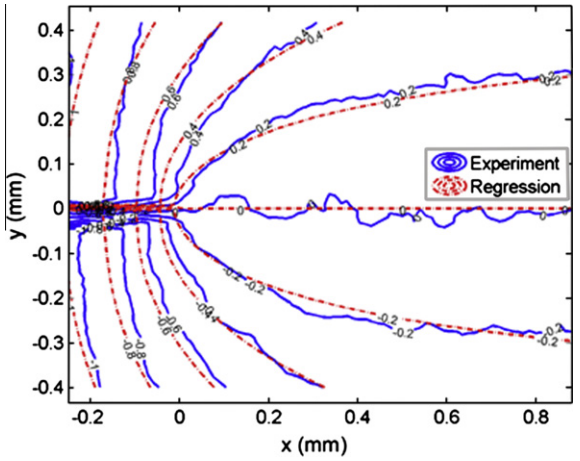

Fig. 6. Comparison of experimentally measured and regression vertical displacement contours in micrometers for the polycrystalline specimen with a crack length of 0.856 mm and a ΔK_I value of 8.01 MPa $\sqrt{}$m found from regression.

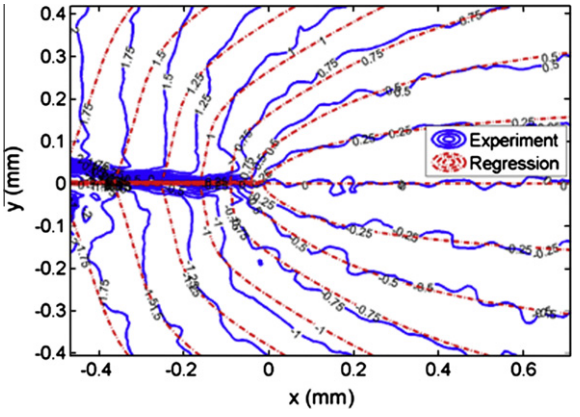

Fig. 7. Comparison of experimentally measured and regression vertical displacement contours in micrometers for the [001] oriented single crystal. The crack length is 1.154 mm with a corresponding ΔK_I regression value of 9.06 MPa $\sqrt{}$m.

Please cite this article in press as: Pataky GJ et al. Full field measurements of anisotropic stress intensity factor ranges in fatigue. Engng Fract Mech (2012), http://dx.doi.org/10.1016/j.engfracmech.2012.06.002

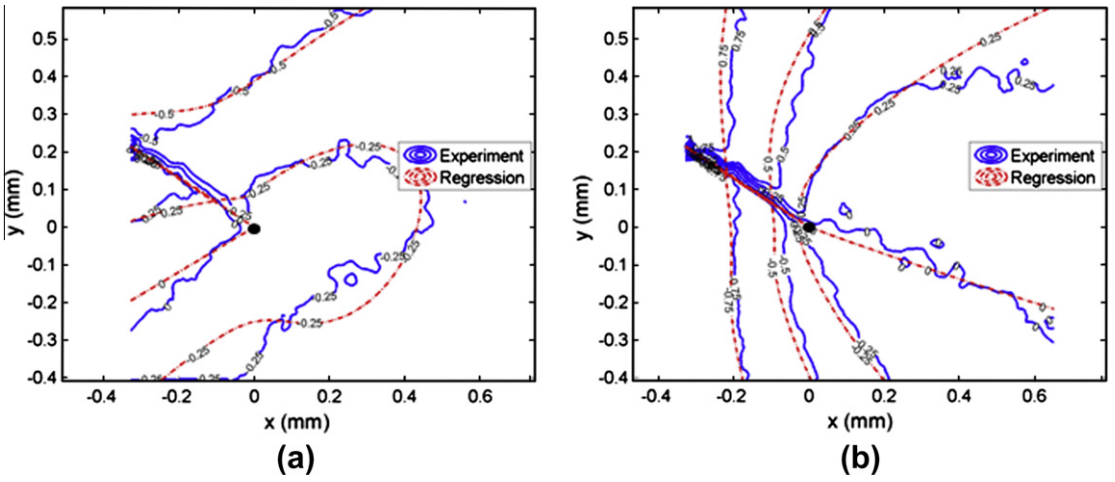

Fig. 8. Comparison of experimentally measured and regression (a) horizontal and (b) vertical displacement contours in micrometers for the [1 1 1] oriented single crystal with a load ratio of $R = 0.05$. The crack is 1.588 mm long with corresponding regression values for ΔK_I of 9.14 MPa $\sqrt{}$m and ΔK_{II} of 4.33 MPa $\sqrt{}$m. The black dot signifies the crack tip location.

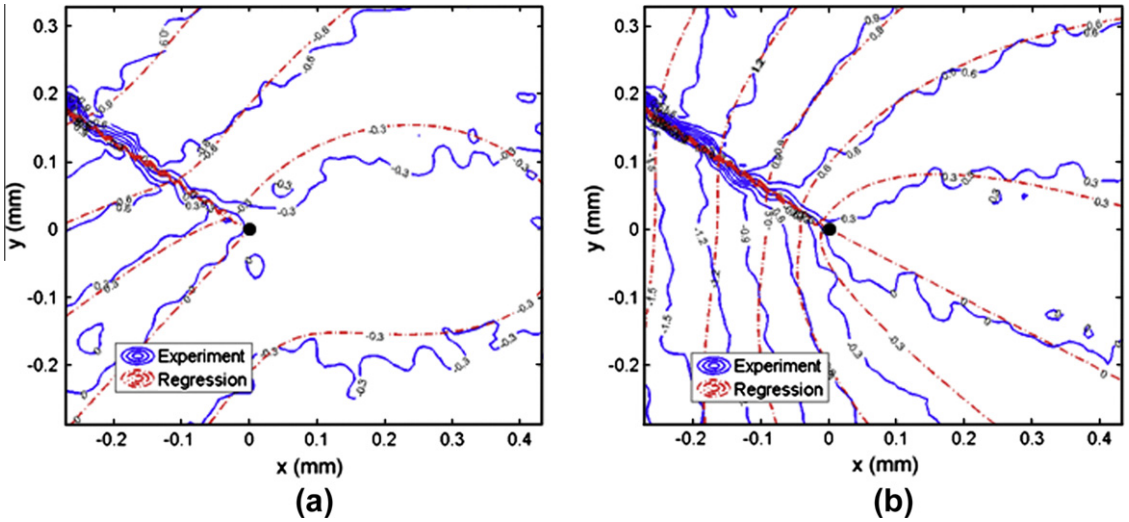

Fig. 9. Comparison of experimentally measured and regression (a) horizontal and (b) vertical displacement contours in micrometers for the [1 1 1] oriented single crystal with a load ratio of $R = -1$. The crack is 1.176 mm long with corresponding regression values for ΔK_I of 20.99 MPa $\sqrt{}$m and ΔK_{II} of 8.49 MPa $\sqrt{}$m. The black dot signifies the crack tip location.

zone area is only 0.0004 mm^2. The maximum plastic zone area for this specimen, 0.0527 mm^2, is a quarter the size of the polycrystalline case, and the DIC strains show a more compact concentration.

The K_{II} component in the two [1 1 1] crystals caused the plastic zone shape to be asymmetric. In the specimen tested at the load ratio, R, of 0.05, the plastic zone shape was a combination of the polycrystalline and [0 0 1] plastic zone shapes as shown in Fig. 12. The upper half of the plastic zone has a shape similar to the smooth, round polycrystalline shape, but the lower half has the more pinched lobe shape of the [0 0 1] specimen. The plastic zone is larger above the crack tip, which is consistent with the displacements that were greater above the crack, as shown in Fig. 8a. The strains were lower for both the polycrystalline and [0 0 1] cases and the gradient was also steeper; outside the direct vicinity of the crack tip, the strains were consistently 0.05% or less. The plastic zone area progression was similar to that of the polycrystalline sample and the maximum area found was 0.1680 mm^2. In the load ratio, R, of -1 [1 1 1] specimen, the plastic zone had a shape similar to the first [1 1 1] specimen and the plastic zone size was the largest found in this study, as displayed in Fig. 13. At 51% of the load, the area was 0.1430 mm^2, which was on the order of the previous [1 1 1] specimen and the polycrystalline specimen at maximum load. Strains greater than 1.1% were measured near the crack tip and the strains were observed to extend farther out from the crack tip vicinity than in the [1 1 1] specimen with the load ratio, R, of 0.05. The strains extend at approximately 30° to

Please cite this article in press as: Pataky GJ et al. Full field measurements of anisotropic stress intensity factor ranges in fatigue. Engng Fract Mech (2012), http://dx.doi.org/10.1016/j.engfracmech.2012.06.002

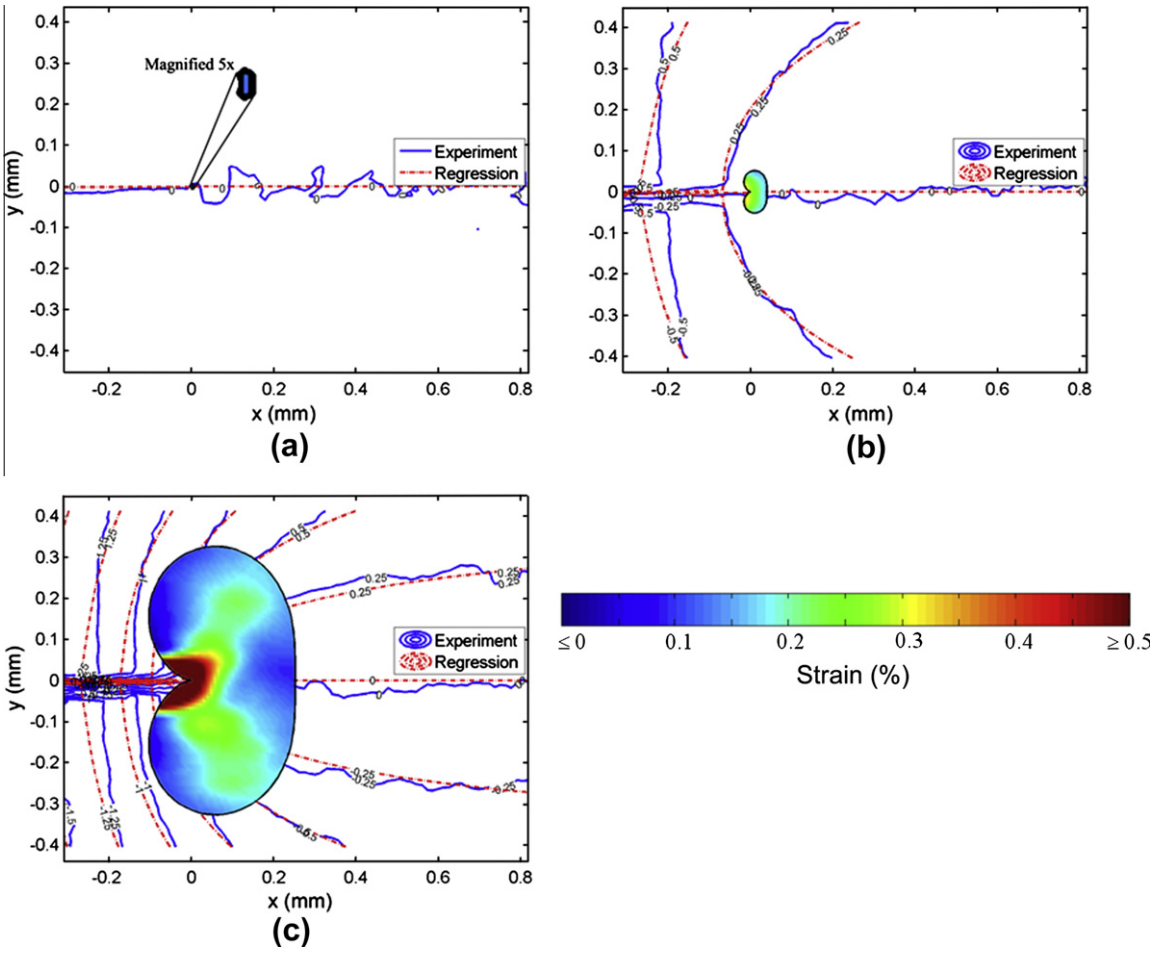

Fig. 10. Plastic zones and vertical displacement contours in micrometers associated with a fatigue cycle of the polycrystalline specimen with a crack length of 0.917 mm and a stress intensity range of $\Delta K_I = 8.34$ MPa $\sqrt{}$m. Each figure represents a different load level during the loading portion of the cycle: (a) 6% with a plastic zone area of $A_{rp} = 0.0007$ mm^2 (b) 43% with a plastic zone area of $A_{rp} = 0.0048$ mm^2 and (c) maximum load with a plastic zone area of $A_{rp} = 0.1920$ mm^2. Strains found from DIC are shown inside each plastic zone.

Table 5
Comparison of effective and classical mode I and mode II stress intensity factors for {1 1 1} oriented specimen loaded at $R = 0.05$.

Crack length (mm)	K_I[a]	$K_{I,eff}$[b]	% Deviation	K_{II}[a]	$K_{II,eff}$[b]	% Deviation
1.378	7.82	6.62	15	5.52	2.89	48
1.484	8.12	7.07	13	5.72	2.83	51
1.552	8.30	6.71	19	5.85	3.98	32
1.699	8.68	7.21	17	6.13	3.74	39
1.940	9.28	8.25	11	6.54	4.48	32

[a] Isotropic estimate.
[b] Anisotropic and closure corrected from regression).

the crack plane below the crack and 60° to the crack plane above the crack. At maximum load, the plastic zone area dominated the entire crack tip region. The greater amount of strain in the load ratio, R, of −1 [1 1 1] single crystal indicates that introducing a compression portion to the fatigue cycle is more damaging than pure tension. This is attributed to the crack opening earlier in the cycle.

It has been recognized that there are additional methods to describing the plastic zone in single crystals. A double slip analysis, which considers only limited slip in a single grain, has been used to describe the effects that crystallographic orientation has on the size and shape of the plastic zone [41]. With the 316L stainless steel being an fcc material, the [1 1 1] single crystals have up to 6 slip systems active and the [0 0 1] single crystal had up to 8 slip systems active. Based on this knowledge, there was significant slip to warrant the use of a continuum model such as Hill's yield criterion.

Please cite this article in press as: Pataky GJ et al. Full field measurements of anisotropic stress intensity factor ranges in fatigue. Engng Fract Mech (2012), http://dx.doi.org/10.1016/j.engfracmech.2012.06.002

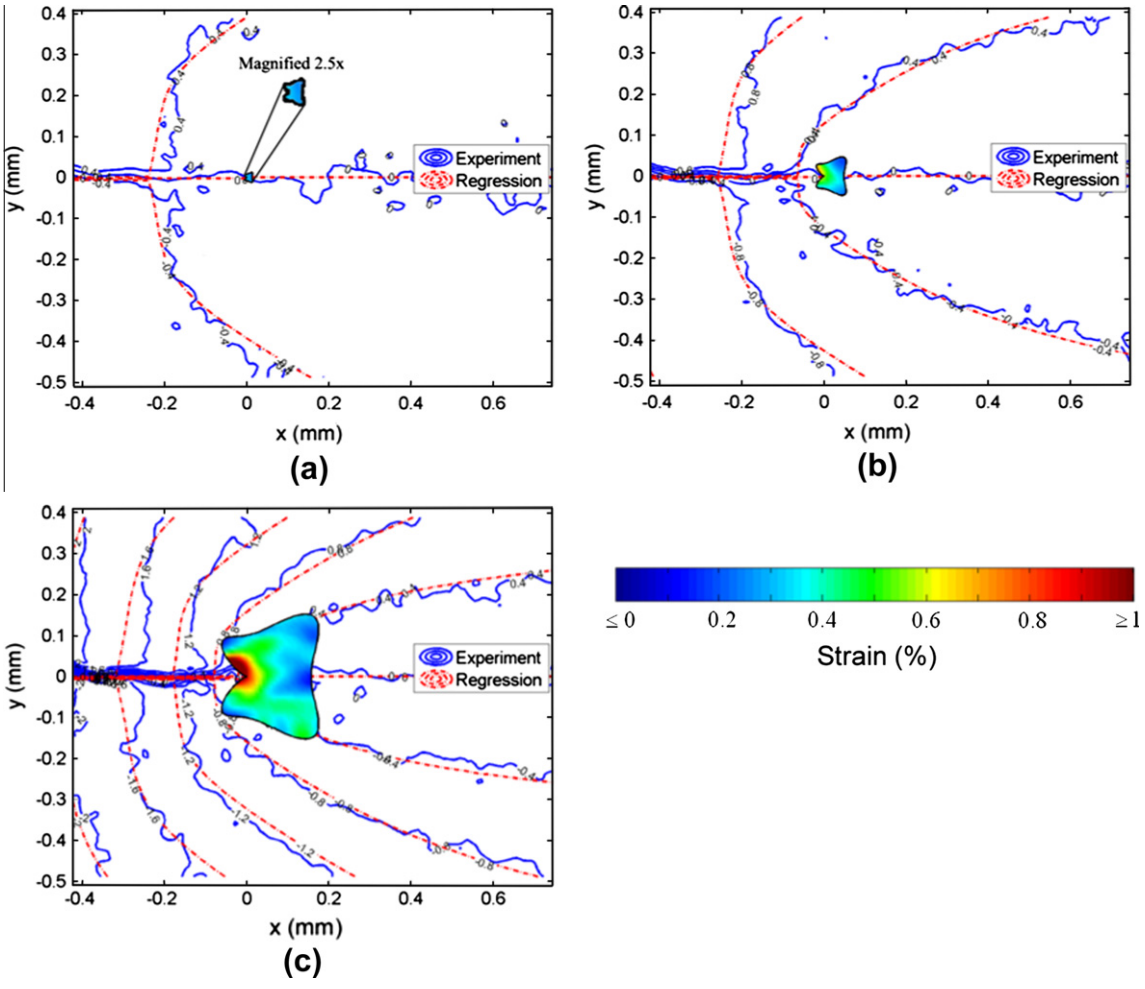

Fig. 11. Plastic zones and vertical displacement contours in micrometers associated with a fatigue cycle of the [0 0 1] oriented specimen with a crack length of 1.174 mm and a stress intensity range of $\Delta K_I = 10.33$ MPa $\sqrt{m}$. Each figure represents a different load level during the loading portion of the cycle: (a) 29% with a plastic zone area of $A_{rp} = 0.0004$ mm^2 (b) 56% with a plastic zone area of $A_{rp} = 0.0050$ mm^2 and (c) maximum load with a plastic zone area of $A_{rp} = 0.0527$ mm^2. Due to the anisotropy of the single crystal, the plastic zone, with DIC strains shown inside, has an irregular shape but is still symmetric due the specimen experiencing pure mode I loading conditions.

5.3. Irreversibility of crack tip strains

Fatigue crack growth is caused by dislocations being emitted from the crack tip during loading, and not fully reversing during unloading, advancing the crack [33]. The residual plastic strain left due to this interaction is the slip irreversibility and has been related to crack propagation [34]. An estimation of the slip irreversibility was determined by finding the amount of irreversible strain accumulated near the crack tip during a fatigue cycle. The schematics in Fig. 14 indicate when the strains were measured during the loading cycle. In Fig. 14a, minimum load is point A, which corresponds to the minimum stress in Fig. 14b. Point B represents the maximum load, halfway through the loading cycle. As the specimen is unloaded, the stress returns to the minimum load, shown in Fig. 14a, irreversible slip has accumulated and the minimum strain has increased to point C in Fig. 14b.

The strains at the two minimum points during the loading cycles were measured for selected crack lengths in each of the four specimens. The results in the axial strain differences at the crack tips are presented in Fig. 14. The inequality between the strain values of the fatigue cycle minimums revealed unrecovered strains, and thus irreversibility. It is observed that the [1 1 1] specimen with a load ratio, R, of -1 had the greatest differences in the axial strain. The [1 1 1] specimen with a load ratio, R, of 0.05 the second highest slope of irreversibility, but it was not significantly higher than the polycrystalline and [0 0 1] specimens. The shear strain irreversibility was also measured. For both the pure mode I growth tests in the polycrystalline and [0 0 1] specimens, the shear strain was negligible to the axial strain. The [1 1 1] specimen with a load ratio, R, of –1 again had a much greater slope than the load ratio, R, of 0.05 specimen, but both specimens had shear strain irreversibilities on the order of the axial strain differences. This again showed the significance of the mode II growth and the damaging effects of a compressive portion of a fatigue cycle for a mixed mode crack (see Fig. 14).

Please cite this article in press as: Pataky GJ et al. Full field measurements of anisotropic stress intensity factor ranges in fatigue. Engng Fract Mech (2012), http://dx.doi.org/10.1016/j.engfracmech.2012.06.002

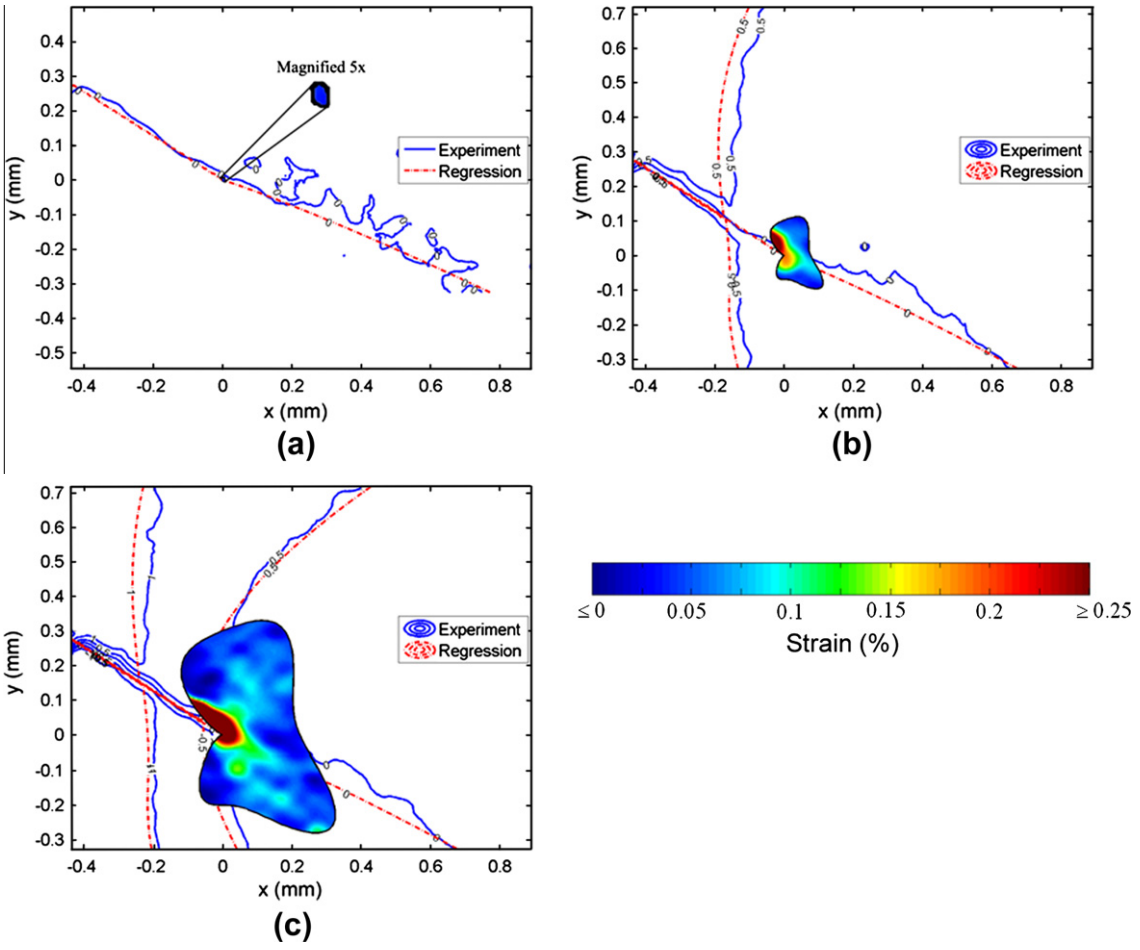

Fig. 12. Plastic zones and vertical displacement contours in micrometers associated with a fatigue cycle of the [1 1 1] oriented specimen at the crack length of 1.716 mm with a load ratio of $R = 0.05$ and stress intensity ranges of $\Delta K_I = 11.91$ MPa $\sqrt{}$m and $\Delta K_{II} = 5.47$ MPa $\sqrt{}$m. Each figure represents a different load level during the loading portion of the cycle: (a) 15% with a plastic zone area of $A_{rp} = 0.0008$ mm^2 (b) 58% with a plastic zone area of $A_{rp} = 0.0196$ mm^2 and (c) maximum load with a plastic zone area of $A_{rp} = 0.1680$ mm^2. The plastic zone size and DIC strains within are asymmetric due to the specimen being under mixed mode loading conditions.

6. Summary

The stress intensity factors, K_I and K_{II}, at the crack tip of polycrystalline and anisotropic single crystal specimens, which were cyclically loaded, were determined using full field DIC displacements. The DIC data was analyzed using a least-squares regression and several observations were made concerning this technique. Since the mode I vertical displacements have symmetry across the crack, it is expected that there be zero vertical displacement in front of the crack tip. When only one set of the DIC displacements (horizontal or vertical only) was used in the regression analysis, the regressed vertical displacement contours took an irregular shape and had nonzero displacements ahead of the crack tip. This was a key indication to the overestimation and underestimation of the stress intensity factor ranges mentioned in Section 3. This reinforces the requirement that both sets of displacements must be used to accurately describe the stress intensity factors in mixed mode fatigue crack loading. The simultaneous use of both stress intensity factors is also observed in Eqs. (14) and (15) where both K_I and K_{II} are used to find each of the energy release rates.

The ability to efficiently determine both sets of displacements at once throughout the entire loading cycle and then the corresponding stress intensity factor ranges in a single crystal is important for furthering the knowledge about Stage I fatigue crack growth. Using experimentally found displacements, crack closure is already included in these stress intensity factors. Stage I fatigue crack growth is dominated by slip, and since the single crystals exhibit anisotropic properties, the stress intensity factor range is highly dependent on the orientation. This was demonstrated with the pure mode I growth in the polycrystalline and [0 0 1] oriented crystal and the mixed mode growth in the two [1 1 1] oriented crystals.

The utilization of digital image correlation also provides for the strains around the crack tip. The plastic zone was determined using the stress field associated with the K_I and K_{II} values obtained from the regression analysis, and the development

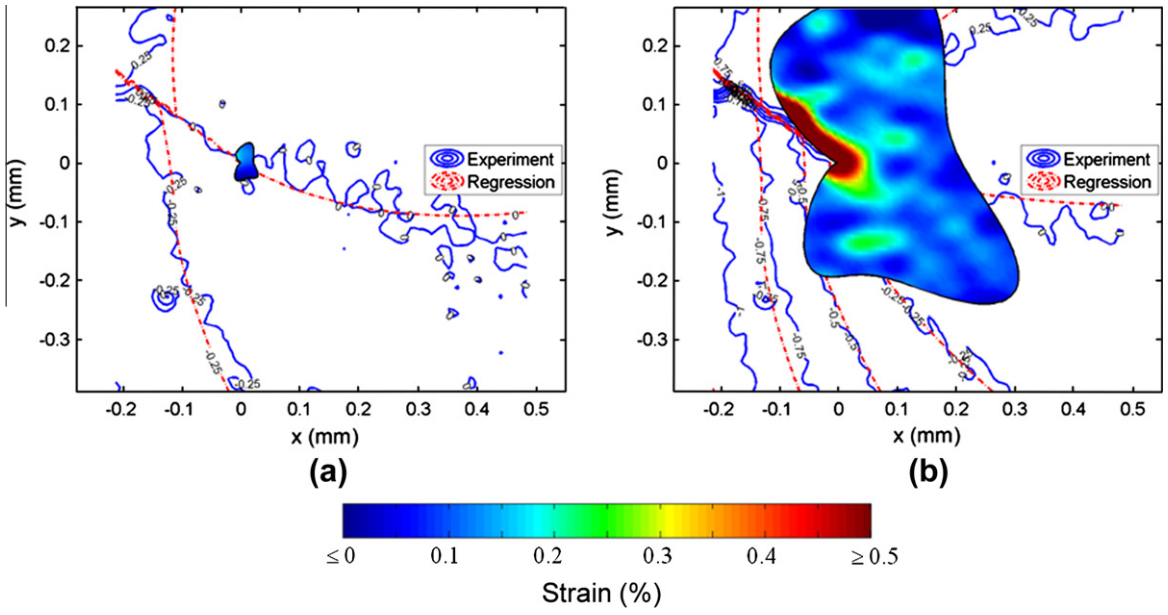

Fig. 13. Plastic zones and vertical displacement contours in micrometers associated with a fatigue cycle of the [1 1 1] oriented specimen at a crack length of 1.024 mm with a load ratio of $R = -1$ and stress intensity ranges of $\Delta K_I = 22.84$ MPa $\sqrt{}$m and $\Delta K_{II} = 9.61$ MPa $\sqrt{}$m. Each figure represents a different load level during the loading portion of the cycle: (a) 15% with a plastic zone area of $A_{rp} = 0.0018$ mm^2 and (b) 51% with a plastic zone area of $A_{rp} = 0.1430$ mm^2. At maximum load, the plastic zone engulfs the entire crack tip region and has been excluded. Asymmetry in the plastic zone and DIC strains is observed due to the mixed mode loading.

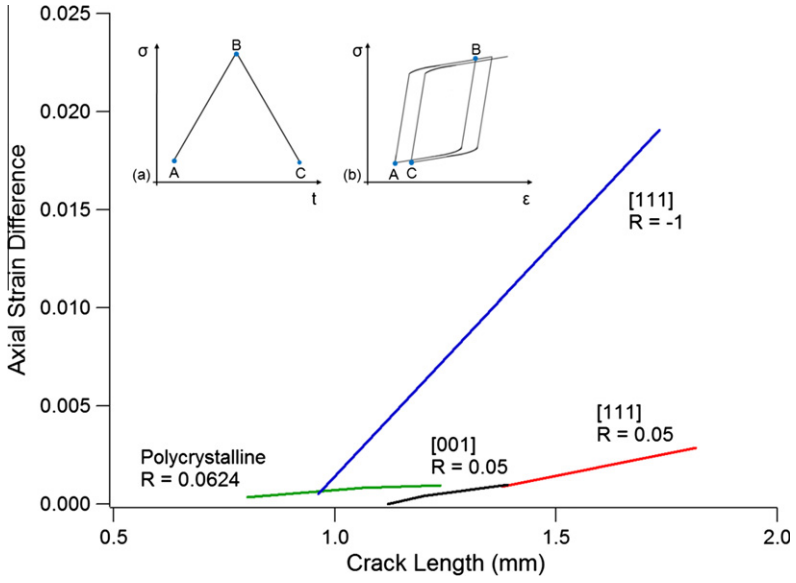

Fig. 14. (a) The fatigue loading cycle as a function of time showing A and C at minimum load. (b) Schematic showing the slip irreversibility between points C and A. Tensile crack tip strain differences between minimum load points (A and C) of selected fatigue cycles as a function of crack length for the four 316L stainless steel fatigue crack growth specimens.

of the strain field inside the plastic zone was observed. By comparing polycrystalline and single crystal specimens, further insight can be gained on how grain boundaries and anisotropy affect the plasticity ahead of a crack tip. When studying mixed mode cases, the effects that varying angles of crack growth have on the asymmetry of the plastic zone and strain development can be determined. By testing using different load ratios, R, the most damaging cases in terms of the plasticity around the crack tip was investigated as seen with the two [1 1 1] specimens. The case with the load ratio, R, of -1 was observed to be the more damaging case due to the compressive portion of the cycle and greater crack opening displacements.

Please cite this article in press as: Pataky GJ et al. Full field measurements of anisotropic stress intensity factor ranges in fatigue. Engng Fract Mech (2012), http://dx.doi.org/10.1016/j.engfracmech.2012.06.002

The strains ahead of the crack tip were quantitatively measured and the slip irreversibility for each cycle was found. This ability can be used to increase the accuracy in crack growth models since the slip irreversibility and crack growth rate are related [34]. A correlation between the increase in slip irreversibility as the crack length increased was observed in each specimen tested. The rate at which each of these increased varied between the polycrystalline specimen and each single crystal orientation tested.

7. Conclusions

The main contribution of this work is the analysis of mixed mode crack growth in single crystal 316L stainless steel.

(1) A least-squares regression technique was developed to find the stress intensity factors and T-stress in both isotropic and anisotropic materials using displacements found from digital image correlation.
(2) The development of the plastic zone size and shape, and the associated strain fields were found for the entire fatigue loading cycle of polycrystalline and single crystal 316L stainless steel specimens.
(3) A quantitative value of the slip irreversibility ahead of the fatigue crack tip was measured and a trend of increasing slip irreversibility with greater crack length was found.

Acknowledgements

The research was supported by a Critical Research Initiative (CRI) at the University of Illinois and partly by the US Department of Energy Nuclear Energy University Program (NEUP) under Grant DOE-INL-00091210.

References

[1] Forsyth PJE, Ryder DA. Some results of examination of aluminium alloy specimen fracture surfaces. Metallurgia 1961;63:117.
[2] Tanaka K. Fatigue crack propagation from a crack inclined to the cyclic tensile axis. Engng Fract Mech 1974;6:493.
[3] Suresh S. Fatigue of materials. Cambridge, UK: Cambridge University Press; 1991.
[4] Smith EW, Pascoe KJ. Fatigue crack initiation and growth in a high-strength ductile steel subject to in-plane biaxial loading, vol. 853. ASTM STP; 1985. p. 111.
[5] Keer LM, Bryant MD, Haritos GK. Subsurface and surface cracking due to Hertzian contact. Trans ASME J Lubr Technol 1982;104:347.
[6] Clayton P, Allery MBP. Metallurgical aspects of surface damage problems in rails. Can Metall Q 1980;21:31.
[7] Duquette D, Gell M. The effects of environment on the elevated temperature fatigue behavior of nickel-base superalloy single crystals. Metall Mater Trans B 1972;3:1899.
[8] Williams ML. On stress distribution at base of stationary crack. Am Soc Mech Eng Trans J Appl Mech 1957;24:109.
[9] Sih GC, Paris PC, Irwin GR. On cracks in rectilinearly anisotropic bodies. Int J Fract Mech 1965;1:189.
[10] Liu HW. Shear fatigue crack growth: a literature survey. Fatigue Fract Engng Mater Struct 1985;8:295.
[11] Rybicki EF, Kanninen MF. A finite element calculation of stress intensity factors by a modified crack closure integral. Engng Fract Mech 1977;9:931.
[12] Nakagaki M, Atluri SN. Elastic–plastic analysis of fatigue crack closure in modes I and II. AIAA J 1980;18:1110.
[13] Smith MC, Smith RA. Toward an understanding of mode II fatigue crack growth, vol. 924. ASTM STP; 1988. p. 260.
[14] Kibey S, Sehitoglu H, Pecknold DA. Modeling of fatigue crack closure in inclined and deflected cracks. Int J Fract 2004;129:279.
[15] Riddell WT, Piascik RS, Sutton MA, Zhao W, McNeill SR, Helm JD. Determining fatigue crack opening loads from near-crack-tip displacement measurements, vol. 1343. ASTM STP; 1999. p. 157.
[16] Sutton MA, Zhao W, McNeill SR, Helm JD, Piascik RS, Riddell WT. Local crack closure measurements: development of a measurement system using computer vision and a far-field microscope, vol. 1343. ASTM STP; 1999. p. 145.
[17] McNeill SR, Peters WH, Sutton MA. Estimation of stress intensity factor by digital image correlation. Engng Fract Mech 1987;28:101.
[18] Carroll J, Efstathiou C, Lambros J, Sehitoglu H, Hauber B, Spottswood S, et al. Investigation of fatigue crack closure using multiscale image correlation experiments. Engng Fract Mech 2009;76:2384.
[19] Anderson TL. Fracture mechanics: fundamentals and applications. 2nd ed. Boca Raton: CRC Press; 1994.
[20] Yoneyama S, Morimoto Y, Takashi M. Automatic evaluation of mixed-mode stress intensity factors utilizing digital image correlation. Strain 2006;42:21.
[21] Abanto-Bueno J, Lambros J. Experimental study of mixed mode crack initiation growth in functionally graded materials. Exp Mech 2006;46:179.
[22] Irwin GR. Analysis of stresses and strains near the end of a crack traversing plate. Am Soc Mech Eng Trans J Appl Mech 1957;24:361.
[23] Nowack H, Trautmann KH, Schulte K, Luetjering G. Sequence effects on fatigue crack propagation; mechanical and microstructural contributions. ASTM Special Technical Publication; 1979. p. 36.
[24] Lankford J, Davidson DL, Chan KS. Influence of crack tip plasticity in the growth of small fatigue cracks. Metall Trans A Phys Metall Mater Sci 1984;15A:1579.
[25] Zhang JP, Venugopalan D. Effects of notch radius and anisotropy on the crack tip plastic zone. Engng Fract Mech 1987;26:913.
[26] Xin G, Hangong W, Xingwu K, Liangzhou J. Analytic solutions to crack tip plastic zone under various loading conditions. Eur J Mech A/Solids 2010;29:738.
[27] Gao H, Alagok N, Brown MW, Miller KJ. Growth of fatigue cracks under combined mode I and mode II loads, vol. 853. ASTM STP; 1985. p. 184.
[28] Betegon C, Hancock JW. Two-parameter characterization of elastic–plastic crack-tip fields. Trans ASME J Appl Mech 1991;58:104.
[29] McClung RC, Sehitoglu H. On the finite element analysis of fatigue crack closure – 2. Numerical results. Engng Fract Mech 1989;33:253.
[30] Tomkins B. Fatigue crack propagation – an analysis. Philos Mag 1968;18:1041.
[31] Brown MW, Miller KJ. Mode I fatigue crack growth under biaxial stress at room and elevated temperature, vol. 853. ASTM STP; 1985. p. 135.
[32] McEvily Jr AJ, Boettner RG. On fatigue crack propagation in F.C.C. metals. Acta Metall 1963;11:725.
[33] Fong C, Tromans D. High frequency stage I corrosion fatigue of austenitic stainless steel (316L). Metall Mater Trans A 1988;19:2753.
[34] Wu X, Koul A, Krausz A. A transgranular fatigue crack growth model based on restricted slip reversibility. Metall Mater Trans A 1993;24:1373.
[35] Sutton MA, Wolters WJ, Peters WH, Ranson WF, McNeill SR. Determination of displacements using an improved digital correlation method. Image Vis Comput 1983;1:133.
[36] Sutton M, Orteu J-J, Schreier H. Image correlation for shape motion and deformation measurements: basic concepts, theory and applications. Spring Media; 2009.

Please cite this article in press as: Pataky GJ et al. Full field measurements of anisotropic stress intensity factor ranges in fatigue. Engng Fract Mech (2012), http://dx.doi.org/10.1016/j.engfracmech.2012.06.002

[37] Shah PD, Tan CL, Wang X. T-stress solutions for two-dimensional crack problems in anisotropic elasticity using the boundary element method. Fatigue Fract Engng Mater Struct 2006;29:343.
[38] Ledbetter HM. Monocrystal elastic constants in the ultrasonic study of welds. Ultrasonics 1985;23:9.
[39] Hill R. Mathematical theory of plasticity. UK: Oxford; 1950.
[40] Bathias C, Pelloux R. Fatigue crack propagation in martensitic and austenitic steels. Metall Mater Trans B 1973;4:1265.
[41] Gall K, Sehitoglu H, Kadioglu Y. Plastic zones and fatigue-crack closure under plane-strain double slip. Metall Mater Trans A 1996;27A:3491.

Please cite this article in press as: Pataky GJ et al. Full field measurements of anisotropic stress intensity factor ranges in fatigue. Engng Fract Mech (2012), http://dx.doi.org/10.1016/j.engfracmech.2012.06.002